SipamMar: a Brazilian autonomous system for oil spill detection and modeling

SipamMar: um sistema autônomo brasileiro de detecção e modelagem de manchas de óleo

SipamMar: un sistema autónomo brasileño de detección y modelado de manchas de petróleo

SipamMar : un système autonome brésilien de détection et de modélisation des nappes de pétrole

Received: 16 July 2025 **Accepted:** 22 September 2025

*Ariel de Almeida Horst Gamba**
*Luis Felipe Ferreira de Mendonça***
*Carlos Alessandre Domingos Lentini****
*Syumara Queiroz de Paiva e Silva*****
*David Oliveira Silva******
*Marcos Reinan de Assis Conceição*******
*André Telles da Cunha Lima********

Abstract
This paper introduces SipamMar, an autonomous Brazilian system designed for the detection and dispersion simulation of oil spills within Brazilian jurisdictional waters. This system aims to enhance the environmental monitoring of the "Blue Amazon," a strategic national asset

* Bachelor's degree in Geology (UnB, 2022). Currently, he holds the position of Analyst in Science and Technology, in the Blue Amazon Coordination, at the Management and Operational Center of the Amazon Protection System (CENSIPAM).

** PhD in Remote Sensing (UFRGS, 2017). Master's degree in Remote Sensing (UFRGS, 2013). Bachelor's degree in Oceanography (FURG, 2010). Adjunct Professor at the Federal University of Bahia (UFBA).

*** PhD in Physical Oceanography and Meteorology from the Rosenstiel School of Marine, Atmospheric, and Earth Science at the University of Miami (RSMAS/UM - USA). Master's degree in Oceanography (USP, 1997).

**** PhD in Oceanography (UFPE, 2024). Master's degree in Oceanography (UFPE, 2020). Collaborating researcher at LMI TAPIOCA (Tropical Atlantic Interdisciplinary Laboratory on Physical, Biogeochemical, Ecological and Human Dynamics) and the Center for Studies and Tests in Risk and Environmental Modeling.

***** Undergraduate student in Computer Engineering (UFBA). Member of the Satellite Oceanography Laboratory (UFBA). Researcher in Remote Sensing applying Machine Learning techniques.

****** Bachelor's degree in Geophysics (UFBA, 2021). Currently, he holds the position of Data Scientist at PETROBRAS.

******* PhD in Physics (PUC-Rio, 2005). Master's degree in Physics (UERJ, 2000). Associate Professor at the Federal University of Bahia (UFBA).

vulnerable to oil spills. SipamMar integrates remote sensing, artificial intelligence, and numerical modeling to establish an automated, operational alert and oil spill simulation framework. Its methodology features automated slick detection in Sentinel-1 Synthetic Aperture Radar (SAR) imagery using a Convolutional Neural Network (U-Net with a ResNet-50 backbone) trained on 8,072 samples. For dispersion modeling, the system employs the Lagrangian MEDSLIK-II model, which is driven by metoceanographic data from Copernicus, ERA5, and GFS/NOAA. To validate detections and minimize false positives, auxiliary environmental data — including wind, chlorophyll, currents, and temperature — are incorporated. Case studies have demonstrated the system's capability to effectively identify oil slicks with a high degree of probability (>80%) and simulate their trajectories within an operational timeframe. SipamMar marks a significant advancement in environmental emergency response, with future work focused on *in-situ* validation and operational expansion for continuous improvement.

Keywords: Oil Spill; Blue Amazon; Remote Sensing; Artificial Intelligence; SAR.

Resumo

O presente artigo descreve o SipamMar, um sistema autônomo brasileiro de detecção e simulação da dispersão de manchas de óleo em águas jurisdicionais brasileiras, visando contribuir para o monitoramento ambiental da Amazônia Azul – patrimônio estratégico e vulnerável a derramamentos de óleo. O sistema integra sensoriamento remoto, inteligência artificial e modelagem numérica para criar um sistema operacional automatizado de alerta e simulação da dispersão de óleo em águas brasileiras. A metodologia inclui detecção automatizada de manchas, por Redes Neurais Convolucionais (U-Net com ResNet-50), em imagens de Radar de Abertura Sintética (SAR) do Sentinel-1, treinadas com 8.072 amostras. A modelagem da dispersão utiliza o modelo Lagrangeano MEDSLIK-II, alimentado por dados meteoceanográficos do Copernicus, ERA5 e GFS/NOAA. Dados ambientais auxiliares (vento, clorofila, correntes e temperatura) são usados para validar detecções e reduzir falsos positivos. Os estudos de caso demonstraram a capacidade do sistema em identificar manchas com altas probabilidades (>80%) e simular suas trajetórias, com um tempo de processamento operacional. O SipamMar representa um avanço significativo na resposta a emergências ambientais, com perspectivas de futuras validações *in-situ* e expansão operacional para otimização contínua.

Palavras-Chave: óleo; Amazônia Azul; Sensoriamento Remoto; Inteligência Artificial; SAR.

Resumen

El presente artículo describe SipamMar, un sistema autónomo brasileño para la detección y simulación de la dispersión de manchas de petróleo en aguas jurisdiccionales brasileñas, con el objetivo de contribuir al monitoreo ambiental de la Amazonia Azul, un patrimonio estratégico vulnerable a los derrames de petróleo. El sistema integra teledetección, inteligencia artificial y modelado numérico para crear un sistema operativo automatizado de alerta y simulación de la dispersión de petróleo en aguas brasileñas. La metodología incluye la detección automatizada de manchas, mediante Redes Neuronales Convolucionales (U-Net con ResNet-50), en imágenes de Radar de Apertura Sintética (SAR) del Sentinel-1, entrenadas con 8.072 muestras. El modelado de la dispersión utiliza el modelo Lagrangiano MEDSLIK-II, alimentado por datos meteoceanográficos de Copernicus, ERA5 y GFS/NOAA. Se utilizan datos ambientales auxiliares (viento, clorofila, corrientes y temperatura) para validar las detecciones y reducir los falsos positivos. Los estudios de caso demostraron la capacidad del sistema para identificar

manchas con altas probabilidades (>80%) y simular sus trayectorias en un tiempo de procesamiento operacional. SipamMar representa un avance significativo en la respuesta a emergencias ambientales, con perspectivas de futuras validaciones *in situ* y expansión operativa para una optimización continua.

Palabras Clave: petróleo; Amazonia Azul; Teledetección; Inteligencia Artificial; SAR.

Résumé
Cet article décrit SipamMar, un système autonome brésilien de détection et de simulation de la dispersion des nappes d'hydrocarbures dans les eaux juridictionnelles brésililiennes, visant à contribuer à la surveillance environnementale de l'Amazonie Bleue – un patrimoine stratégique vulnérable aux déversements de pétrole. Le système intègre la télédétection, l'intelligence artificielle et la modélisation numérique pour créer un système opérationnel automatisé d'alerte et de simulation de la dispersion des hydrocarbures dans les eaux brésiliennes. La méthodologie comprend la détection automatisée de nappes par des Réseaux de Neurones Convolutifs (U-Net avec ResNet-50) sur des images de Radar à Synthèse d'Ouverture (RSO) de Sentinel-1, entraînées avec 8 072 échantillons. La modélisation de la dispersion utilise le modèle Lagrangien MEDSLIK-II, alimenté par des données météo-océanographiques de Copernicus, ERA5 et GFS/NOAA. Des données environnementales auxiliaires (vent, chlorophylle, courants et température) sont utilisées pour valider les détections et réduire les faux positifs. Les études de cas ont démontré la capacité du système à identifier les nappes avec de fortes probabilités (>80%) et à simuler leurs trajectoires dans un temps de traitement opérationnel. SipamMar représente une avancée significative dans la réponse aux urgences environnementales, avec des perspectives de validations futures *in situ* et d'expansion opérationnelle pour une optimisation continue**.**

Mots-clés: pétrole ; Amazonie Bleue ; Télédétection ; Intelligence Artificielle ; RSO.

1 INTRODUCTION

Brazil's coastline, stretching over 7,400 kilometers and encompassing 5.7 million km² of Exclusive Economic Zone, nicknamed the "Blue Amazon," constitutes a national asset of strategic interest, both from an economic and national sovereignty perspective, as well as an ecological one. Economically, the Blue Amazon is responsible for 95% of the national oil production and 83% of natural gas production (Andrade; Franco, 2018). Furthermore, from a logistical and commercial standpoint, this immense region contains Brazil's main access routes to global trade. As highlighted by Admiral Eduardo Bacellar Leal Ferreira in 2017, these maritime routes are responsible for 97% of Brazilian foreign trade and more than 90% of the country's communications (Andrade; Franco, 2018).

Not only that, the Blue Amazon also harbors large reserves of minerals crucial for the manufacture of modern technologies, such as rare earth elements (REEs), manganese, iron,

cobalt, among others (Pessoa, 2015). The recent Brazilian claim to the Rio Grande Rise demonstrates the mineral exploration potential of the Blue Amazon (Silva, 2021). On the other hand, maritime traffic and marine resource exploration activities can compromise the marine environment, making this region vulnerable to various activities harmful to the marine ecosystem, such as marine pollution (Barbosa Júnior, 2012). The vulnerability of this vast region to oil spill events was dramatically highlighted by the spill that occurred in northeastern Brazil in 2019, which affected more than 2,800 km of coastline, impacting fragile ecosystems and causing serious socioeconomic and health effects in 11 Brazilian states (Soares *et al.,* 2022; De Moura; Polito, 2022).

The event, to date the largest ever recorded in tropical regions, exposed deficiencies in national environmental surveillance, alert, and response systems (Magris; Giarrizzo, 2020). Given this reality, improving the capacity to monitor and respond to these environmental disasters has become an urgent necessity to preserve the Blue Amazon and the country's coastal regions. However, monitoring the Blue Amazon is challenging, as it faces budgetary and personnel constraints, making surveillance and response capabilities logistically inefficient, relying solely on traditional naval patrol resources.

In this context, the use of remote sensing through satellite imagery has the potential to expand monitoring capacity in this vast area. The use of Synthetic Aperture Radar (SAR) images, for example, allows the detection of objects and events in the ocean without the need for illumination and favorable weather conditions, typical of optical sensors (Mityagina; Lavrova, 2018; Brekke; Solberg, 2005). On the other hand, the quantity of images available and the need for trained technical personnel restrict the use of these technologies to a few professionals.

Faced with these challenges, machine learning (ML) offers tools for the development of autonomous detection and monitoring systems. In simplified terms, ML consists of the ability of computers to reproduce human intellectual operations through algorithms, such as convolutional neural networks, allowing computers to perform tasks that would typically require human intelligence, including learning, reasoning, and decision-making in a short period of time (Ortiz Valadez *et al.*, 2024). In the field of ML, this branch is dedicated to creating systems that learn from data, identify patterns, and make decisions with little or no human intervention (Ortiz Valadez *et al.*, 2024). This unsupervised learning capability is essential for handling large volumes of data generated by remote sensing equipment, such as SAR images.

Deep Learning (DL) is a specialized branch of ML that uses multi-layered neural networks (deep neural networks) to analyze complex data structures (Bhattacharyya *et al.*, 2020). Deep Learning techniques are especially effective in areas with high-dimensional data, such as speech and image recognition, as they allow the model to autonomously identify the features needed to classify or predict from raw data (Lemley *et al.*, 2017). Convolutional Neural Networks (CNNs), for example, which excel in computer vision tasks, are used for object detection in SAR images.

In this context, in order to assist in the environmental monitoring of the Blue Amazon, the project entitled "Research for the Development of an Autonomous System for Oil Detection and Monitoring in the Ocean" was formalized through a Decentralized Execution Agreement between the Management and Operational Center of the Amazon Protection System (CENSIPAM) and the Federal University of Bahia (UFBA). The overall objective of this project is to integrate remote sensing, machine learning, and numerical modeling technologies to design an automated operational system for alerting and simulating the dispersion of oil spills in Brazilian jurisdictional waters: SipamMar. This article presents the architecture of the developed system, highlighting the methodological advances applied to automatic detection by convolutional neural networks and to the predictive modeling of contaminant trajectories. Finally, a typical case study is presented to demonstrate the application of SipamMar as a coastal environmental monitoring system.

2 RELATED WORKS

2.1 MACHINE LEARNING: SPILL DETECTION IN SAR IMAGES

Machine learning is an effective tool to aid in the detection of oil spills in the ocean, especially when combined with Synthetic Aperture Radar (SAR) imagery. SAR technology is advantageous for oil spill detection due to its ability to capture images regardless of weather and lighting conditions (sunlight), enabling continuous ocean monitoring (Topouzelis, 2008).

A number of machine learning-based techniques have been proposed to improve the detection and classification of oil spills in SAR images. For example, DL networks such as ShuffleNet have been used to increase the accuracy of oil spill segmentation in SAR images and reduce speckle noise (inherent to SAR technology) in different cases (Aghaei *et al.*, 2022).

On the other hand, deep networks, such as stacked autoencoders and deep belief networks, have already been used to optimize and classify oil spills more accurately by

extracting and refining polarimetric SAR features (Chen *et al.*, 2017). Furthermore, advanced techniques incorporating comprehensive algorithms can also be applied. These techniques combine dark spot detection in the image, feature extraction, and classification to differentiate between oil spill events and similar phenomena with greater precision (Raeisi *et al*., 2018).

One technique used, among others, to improve this detection process is the use of fuzzy logic algorithms. The purpose of this algorithm is to improve the classification probabilities of oil spills in relation to lookalikes, which are features in the image that resemble oil spills in SAR images, also known as "false positives". This methodology presents a more convenient method for operational purposes, although natural features can still hinder detection (Liu *et al.*, 2010). Therefore, the integration of LM models with SAR images is a suitable and promising methodology for the detection and monitoring of oil spills in the ocean.

2.2 RESTRICTIONS AND DIFFICULTIES IN OIL SPILL DETECTION USING SAR IMAGING

The use of SAR imagery has emerged as an effective tool for monitoring and identifying oil spills, due to its ability to operate in adverse weather conditions and during the day or night. However, despite its advantages, the use of SAR faces restrictions and limitations that can affect its accuracy and reliability.

One of the main difficulties in using SAR for this purpose lies in differentiating oil spills from natural phenomena that present similar visual characteristics, such as biogenic films, calm waters, whirlpools, or areas of low wind speed. These "false positives" (lookalikes) can lead to classification errors and compromise the effectiveness of detection (Liu *et al*., 2010; Zakzouk *et al.*, 2025). It is possible to minimize false positive cases through fuzzy logic algorithms or probabilistic approaches (Liu *et al.*, 2010; Nirchio *et al.*, 2005).

The spatial and temporal resolution of SAR satellites plays a critical role in the detection and monitoring of oil spills. High-resolution SAR images and the imaging of large areas make the large-scale use of SAR technology expensive. For this reason, SAR images are obtained from free sources, such as the Sentinel constellation of the European Space Agency (ESA). Images from the Sentinel-1 satellite, for example, provide a spatial resolution of 10 meters and a revisit capability restricted to 6 days (Zakzouk *et al.*, 2025). Furthermore, the imaging region covered by the satellite is controlled by other organizations, which limits the area effectively monitored.

Finally, speckle noise is an inherent characteristic of SAR imaging caused by the coherent nature of radar signals. This noise, also known as the "salt-and-pepper effect/noise," manifests as granular interference in images that can obscure the image. Although speckle noise is minimized, it still interferes with SAR images (heterogeneous backgrounds and blurred edges), hindering the segmentation and accurate detection of oil spills (Aghaei *et al.*, 2022). These limitations and challenges highlight the continued need to improve analytical methods, as well as the use of complementary data to increase the reliability and accuracy in oil spill detection using SAR technology.

3 METHODOLOGY

3.1 GENERAL SYSTEM ARCHITECTURE

The developed system consists of two main modules: (a) automated detection of oil spills from SAR images, and (b) numerical modeling of oil dispersion based on meteo-oceanographic data and physicochemical characteristics of the oil. Both modules are integrated by automated routines for acquisition, pre-processing, post-processing, simulation, and visualization of results, operating in replicated environments on the CENSIPAM and UFBA servers.

3.2 DETECTION VIA CONVOLUTIONAL NEURAL NETWORKS

Oil spill detection was performed by implementing classifiers based on the U-Net architecture, commonly used in medical image classifiers (Zhou, 2018), and the ResNet-50 architecture as a backbone embedded in the SipamMar platform.

The model was trained using a dataset composed of IW SLC products from the Sentinel-1 A and B satellites, containing cases of possible oil spills in the ocean. These products were compiled by the team at the Satellite Oceanography Laboratory (LOS) of the Federal University of Bahia (UFBA). The raw data were provided by the European Space Agency (ESA), while the identification and validation of spills—confirmed or with a high probability—was carried out using the Sentinel Vision portal and the Marine Pollution Surveillance Report platform, maintained by OSPO (Office of Satellite and Product Operations).

Although the database is constantly expanding, the results presented in this work used a total of 82 Sentinel-1 A and B products. These products were labeled and subsequently cropped into small square images. For this study, only one set of 512 × 512-pixel images was

used, totaling 8,072 samples, half of which showed oil and the other half did not. The evaluation strategy adopted was the *holdout*, with an 80% split for training and 20% for validation.

To avoid overfitting, several regularization techniques were applied, including an L2 (weight decay) penalty with a value of 10^{-2}, and a 10% dropout, inserted in specific layers of the network.

Additionally, the Early Stopping technique was used, which automatically interrupts training if validation loss fails to improve for a certain number of epochs—in this case, a patience of 14 epochs. This technique directly impacts the loss curve, as it can end training before the model enters overfitting, preventing validation loss from forming the typical U-shaped curve. Thus, training is terminated at the point of best validation performance, without allowing the loss to increase again.

Not only that, but the FocalLoss loss function, appropriate for handling imbalances between classes, was also used in the training. The chosen optimizer was Adam, with an initial learning rate of 10^{-5}. A ReduceLROnPlateau type scheduler was also used, which monitors validation loss and automatically reduces the learning rate when the metric shows stagnation or worsens. The patience factor for the scheduler was set to four epochs. This strategy impacts the loss curve by smoothing the descent and contributing to better convergence, even in regions of little variation.

Regarding the programming language, Python was used, with the PyTorch library as the main framework. PyTorch offers native integration with CUDA technology, allowing the use of NVIDIA GPUs to accelerate operations. In this case, two NVIDIA GeForce RTX 3060 cards were used, each with 12 GB of VRAM. The batch size was adjusted based on the available memory limitation, resulting in an approximate value of 18 samples per batch. This number may vary depending on the size of the images, memory usage by other processes, and other factors of the execution environment.

Regarding the programming language, Python was used, with the PyTorch library as the main framework. PyTorch offers native integration with CUDA technology, allowing the use of NVIDIA GPUs to accelerate operations. In this case, two NVIDIA GeForce RTX 3060 cards were used, each with 12 GB of VRAM. The batch size was adjusted based on the available memory limitation, resulting in an approximate value of 18 samples per batch. This number may vary depending on the size of the images, memory usage by other processes, and other factors of the execution environment.

Table 1 - Performance metrics of the U-Net detection model with ResNet-50 as backbone

	LOSS	ACC	PRECISION	RECALL	F1	JACCARD
TRAINING	0.002967	0.999546	0.949419	0.950116	0.949466	0.901332
VALIDATION	0.003385	0.996541	0.950338	0.852389	0.897334	0.815822

Source: Designed by the authors, 2025.

The classifier output is a georeferenced probability mask which, upon exceeding defined thresholds, triggers alerts via email and FTP, accompanied by auxiliary environmental data (e.g., currents, winds, and chlorophyll concentration). Operationally, the complete processing time, from image acquisition to alert issuance, is approximately 25 minutes.

3.3 NUMERICAL MODLING WITH MEDSLIK-II

After the detection of the oil slicks in SAR, the trajectory and transformation of the oil were simulated with MEDSLIK-II, a Lagrangian model widely used for short-term forecasting of sea surface spills due to its robustness, ability to represent different types of oil, and ease of coupling to ocean circulation models (De Dominicis *et al.*, 2013a; 2013b). In MEDSLIK-II, the spill representation combines deterministic processes (advection/diffusion forced by currents and wind) and stochastic processes (random walk associated with turbulent diffusivity), in addition to wind drift and, when configured, Stokes drift associated with the wave field (De Dominicis *et al.*, 2013a).

The model's internal structure organizes the state variables into three interconnected groups: (i) "spill" type variables, which control the volume balance in the thick and thin layers at the surface and subsurface, on which weathering processes act; (ii) "particle" type variables, which carry position, volume (with evaporative and non-evaporative parts) and status (surface, dispersed, sedimented or on shore), responsible for transporting oil in the stream field; and (iii) "structural" variables, which express the concentrations at the surface, in the column and on the shore, used in the generation of spatial products (De Dominicis *et al.*, 2013a). Weathering processes (evaporation, emulsification, dispersion/upwelling, and spreading) follow the family of classic oil fate algorithms, with parameters dependent on wind at 10 m and sea surface temperature (SST), and beaching with residence times adjusted to the type of coast (Mackay et al., 1980; De Dominicis *et al.*, 2013a).

In the operational version of SipamMar, environmental inputs are obtained from consolidated operational sources such as Copernicus Marine Service (current and SST fields), ERA5 and GFS/NOAA (wind), and integrated by Python routines for automated download

(motuclient, cdsapi and requests), pre-processing (standardization/grid, formatting compatible with MEDSLIK-II in NetCDF) and visual validation of forcing factors. This automation also drives the post-processing stage, standardizing the generation of maps and animations and reducing manual intervention during operation, as described in its pipeline (De Dominicis *et al.*, 2013b).

In our operational setup, each simulation is initialized with 100,000 Lagrangian particles distributed over the detection polygons, a solution that offers good spatial resolution of the simulated concentrations and is within the range recommended/validated in the MEDSLIK-II literature itself (De Dominicis *et al.*, 2013a; 2013b). The kinematics are integrated with a fixed time step for transport, while weathering processes use a shorter internal sub-step, according to the model formulation; thus, stability and accuracy control is achieved by choosing the steps and diffusion coefficients (De Dominicis *et al.*, 2013a).

The numerical tolerance of the MEDSLIK-II solver covers the spatial resolution of the oil tracer grid, the time steps, and the diffusion coefficients used. For realistic concentration reconstruction, the oil tracer grid resolution is approximately 100 meters. This resolution is calibrated to be between the diffusion scale (approximately 60 meters) and the advective scale (approximately 180 meters), considering a Lagrangian time step of 1800 seconds (30 min) and a horizontal diffusivity coefficient of 2 m^2/s, consistent with high-resolution Eulerian models (De Dominicis et al., 2013a). The vertical diffusivity coefficients (Kv) are 0.01 m^2/s within the mixing layer and $1x10^{-4}$ m^2/s below it, respectively (De Dominicis *et al.*, 2013b).

The diagnostic outputs of our system are stored in NetCDF every 1 hour, ensuring compatibility with the forcing and the routine for disseminating the results; When necessary for communication, cartographic products are aggregated into wider windows without altering the internal temporal resolution of the calculation (De Dominicis *et al.*, 2013b). The deterministic terms of surface displacement include the contribution of ocean model currents, a wind correction (applicable as an uncertainty term when surface circulation is not fully resolved), and, when enabled, Stokes drift parameterized from the JONSWAP wave spectrum (Hasselmann *et al.*, 1973; De Dominicis *et al.*, 2013a). For latitudes greater than 10°S, a wind drift factor of 6% and an angle of 45° are used, as these were considered the most effective for reproducing the trajectory observed in Brazilian waters, differing from the typical values (1-6% for the factor and 0-25° for the angle) found in other regions such as the Mediterranean wind (Correia Lima *et al.*, 2025).

Together, this configuration closes the operational chain: ingestion of SAR data and automatic detection; preparation of forcings; Lagrangian simulation with weathering and

interaction with the coast; and GIS-ready export (NetCDF and vector layers), which supports the rapid analysis and reproducibility of the system flow, a central foundation of the use cases presented. This makes them crucial tools for supporting decision-making in environmental response and in planning actions to mitigate and prevent oil spills at sea.

The complete automation of the process – from configuration to figure generation – was consolidated by scripts, significantly reducing human intervention and execution time, as well as minimizing configuration errors. The execution time was approximately 20 minutes.

4 DEVELOPMENT

4.1 OPERATIONAL INTEGRATION

The system already operates with automatic Sentinel-1 image ingestion capabilities, neural network analysis, alert transmission, and activation of the ocean modeling module. Meteorological and oceanographic data are acquired programmatically, and simulations are run considering multiple oil types (light, medium, and heavy), with daily graphical outputs and hourly animations for each type.

The decision to run the model for three different oil types was made assuming a lack of API information for the spilled oil, which is quite common in Brazilian basins. This type of information is not openly shared due to "sensitive" issues alleged by operators in Brazilian waters. However, with the specific API, only one simulation is performed. The interoperability of the system outputs with GIS environments allows the generation of analytical products with explicit spatial support, which are fundamental for environmental response and the planning of mitigation and prevention actions.

4.2 CASE STUDY 1: SOUTHWESTERN PORTION OF THE GULF OF MEXICO

To demonstrate the applicability of the developed system, an episode of detection of a possible oil spill identified by Sentinel-1 SAR imagery was selected. These coordinates correspond to the southwestern portion of the Gulf of Mexico, near the coast of the state of Veracruz (Mexico), and the maritime region between the Bay of Campeche and the southern coast of the state of Tamaulipas. This case study illustrates the complete functioning of the operational chain – from image ingestion, through automatic detection, to dispersion simulation and visualization of potential impacts.

Figure 1 - Metadata for the Sentinel-1 SAR image (CC57 orbit) used for automated detection in the Gulf of Mexico

Coord. Range	Minimum	Maximum
Latitude	20.3953	22.505
Longitude	-95.6758	-92.9202

- Input title: `S1A_IW_SLC__1SDV_20200203T002425_20200203T002453_031081_039239_CC57`
- Input path: `/host/mnt/camobi_process/rioss_outputs/prod/data/4dd90752-d616-55df-b420-dc1d35691bd8/preproc_sar/4dd90752-d616-55df-b420-dc1d35691bd8.nc`

Source: SipamMar.

4.2.1 Automated detection

The analyzed SAR image was processed by the SipamMar system, trained with U-Net type convolutional neural networks. Figure 2 shows, in panel (a), the georeferenced Sentinel-1 SAR image (σ_0 in dB) of the southwestern Gulf of Mexico region, without indications of detection, while panel (b) shows the results of the automatic segmentation performed by the SipamMar system.

The spills identified as probable oily features are highlighted with red outlines and numbered according to their respective detection probabilities. Detections occur in areas with low backscattering ($\sigma_0 < -25$ dB), consistent with the suppression of surface roughness caused by oil films. The comparison between the two panels highlights the system's ability to automatically identify suspicious regions in complex SAR images, even over a wide spatial extent and under gradual variation in sea roughness.

Figure 2 - Post-processed and georeferenced CC57 SAR images at σ_0 (Sigma_zero, in dB). (a) SAR image without detections; (b) SAR image with system detections, marked in red

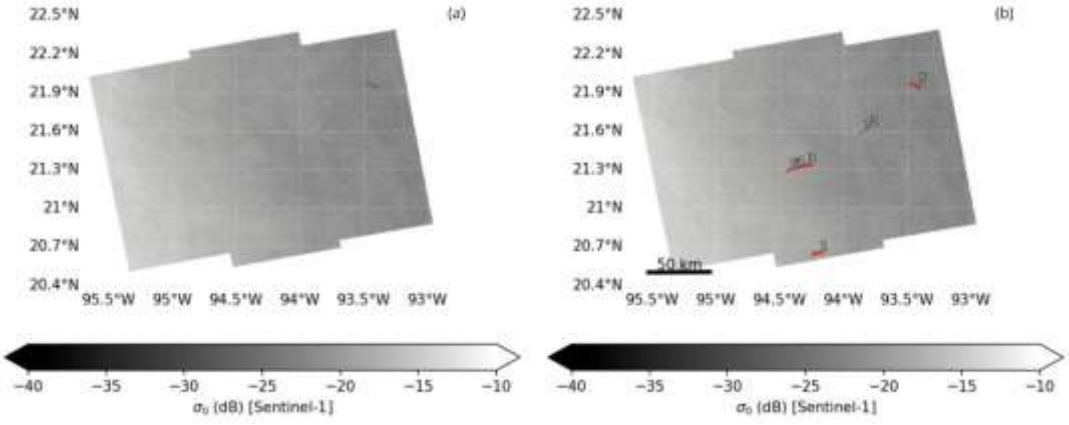

Source: SipamMar

Figure 3 presents the output table of the automatic detection model of the SipamMar system, containing metadata for seven polygons segmented as possible oil spills in the ocean. For each detection, the geographic coordinates (latitude and longitude of the centroid), the estimated area (in km²), the average probability of detection, and the highest probability located within the spill are provided. The average probability values vary between 44% and 60%, with local maximums reaching 84%, indicating different levels of confidence in the detections, with polygon 1 being the most relevant from an operational point of view. The presence of links for quick look allows visual validation of the identified features, reinforcing the integration between automatic processes and analysis by experts. This data is crucial for prioritizing inspections and triggering numerical dispersion modeling.

Figure 3 - Metadata from automatic detections performed by the SipamMar system, indicating location, area, average and maximum probability of oil presence for seven polygons identified in SAR Sentinel-1 imagery

	Latitude	Longitude	Area (km²)	Probability	Highest Probability	Quicklook
1	-94.2051	20.6499	4.234	60%	84%	link
2	-93.8101	21.6269	1.344	53%	79%	link
3	-94.3017	21.3299	2.36	52%	77%	link
4	-94.3912	21.3079	1.558	49%	76%	link
5	-93.4262	21.9534	3.596	47%	77%	link
6	-94.4386	21.2905	0.522	46%	75%	link
7	-93.863	21.5869	0.434	44%	65%	link

Sourse: SipamMar

The network provides two confidence metrics: the average probability of detection across the entire spill and the highest probability located at some point within it. Average probabilities range from 44% to 60%, while maximum values reach up to 84%, strongly suggesting the presence of oil in certain regions. It is important to note that the system only issues alerts when the average probability of detection exceeds the threshold previously defined by the operator, ensuring greater robustness and reducing the emission of false positives.

This data is fundamental for prioritizing field verification actions and for feeding modeling systems of the potential contamination trajectory. Figure 4 shows enlarged cutouts of the identified spills, highlighting well-defined contours and distinct signatures that corroborate the hypothesis of oily contamination. The classification was based on a probability greater than 0.6, a threshold calibrated based on performance metrics of the models in previous campaigns.

Figure 5 represents auxiliary environmental variables that comprise the dataset supporting the validation of automatic oil spill detections performed by the SipamMar system.

The first image shows the chlorophyll-a concentration (mg/m³), revealing low levels in the detection area (values < 1 mg/m³), which reduces the probability that the dark patterns in the SAR image are caused by biogenic films associated with algal blooms. The second figure shows the surface wind speed, with a predominance of values between 5 and 7 m/s, which characterizes conditions favorable to the formation of roughness patterns and the passive dispersion of oil at the air-sea interface.

Figure 4 - Excerpts of the oil slicks, from the CC57 image, detected by the system

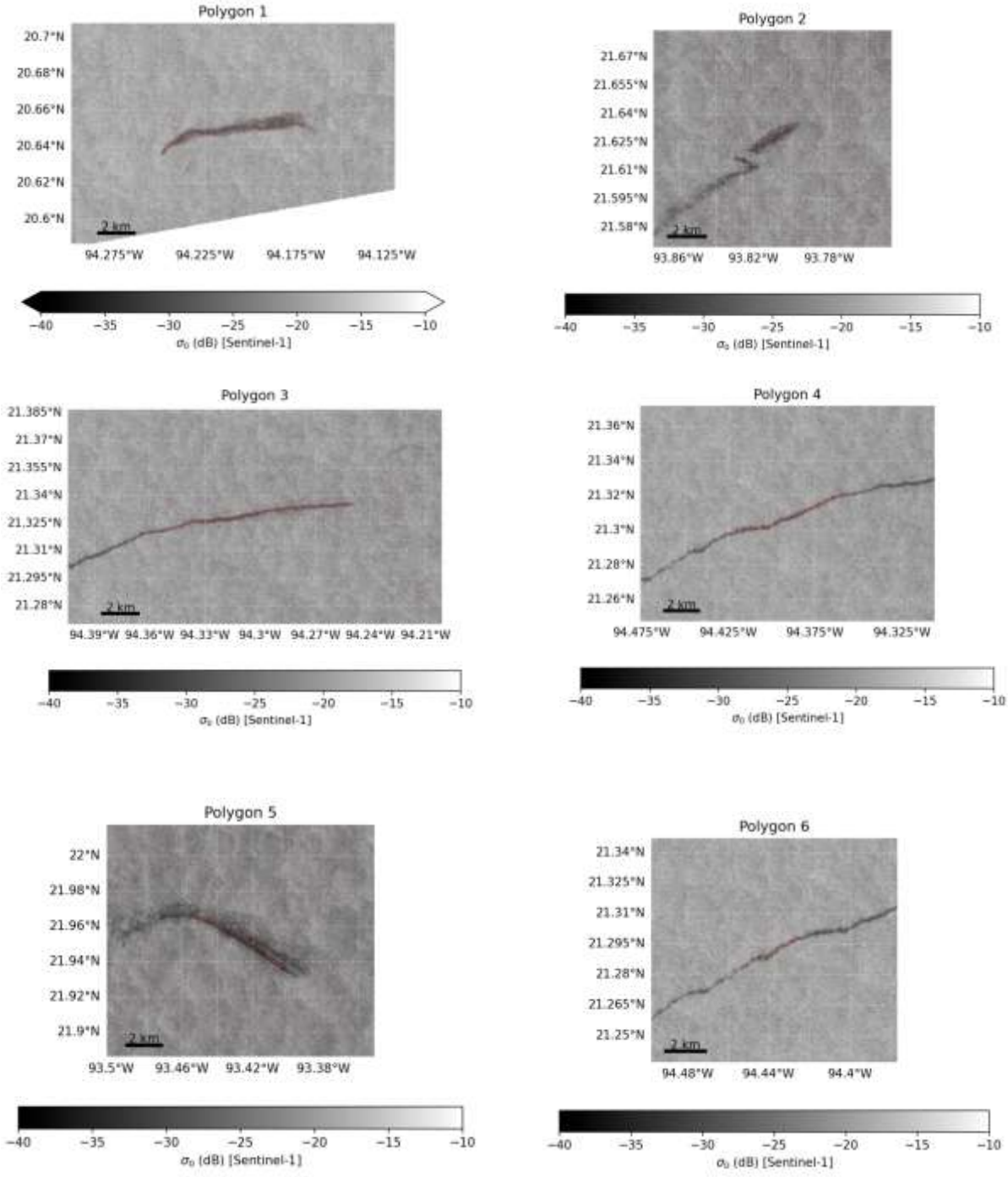

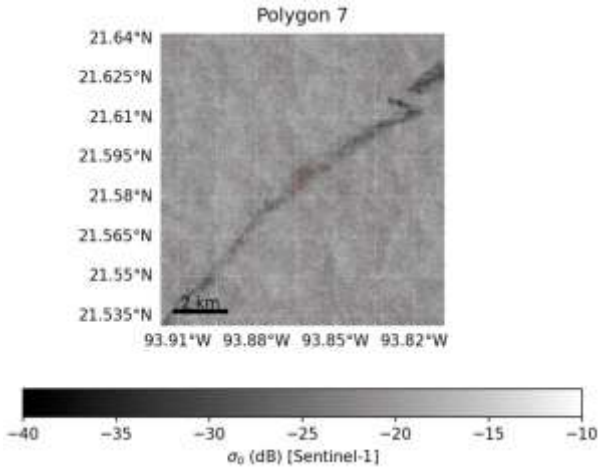

Source: SipamMar.

In the third figure, the speed of surface currents shows regions with intense dynamic activity (values greater than 0.3 m/s), directly influencing the trajectory and fragmentation of the oil slick. Finally, the fourth image shows the sea surface temperature (SST), with homogeneous values between 27°C and 29°C, indicating regional thermal stability. This complementary data is essential for the operator's critical evaluation, allowing them to rule out false detections caused by natural artifacts, confirm the physical consistency of the detected anomalies, and realistically feed oil spill dispersion prediction models.

Figure 5 – Environmental data supporting the validation of oil detections performed by the SipamMar system: (a) chlorophyll-a concentration (mg/m³), (b) surface wind speed (m/s), (c) surface ocean current speed (m/s), and (d) sea surface temperature (°C). These variables support the operator's analysis, helping to distinguish real oil slicks from natural artifacts

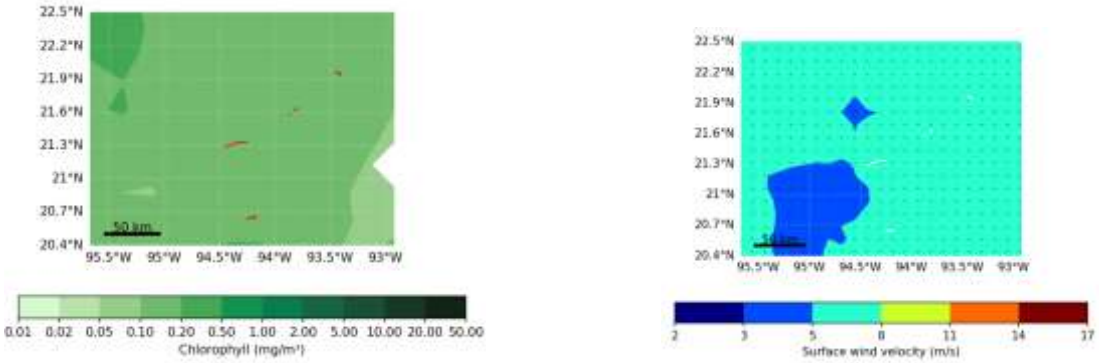

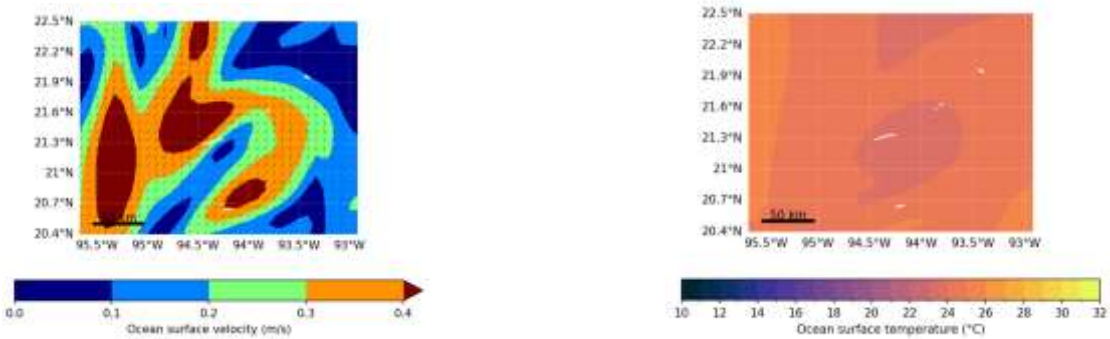

Source: SipamMar.

Chlorophyll, for example, can indicate the presence of biological blooms that alter the characteristics of the sea surface. Conversely, the absence of wind or the presence of pronounced thermal gradients can result in patterns similar to oil spills. Thus, integrating this information into the screening process significantly reduces the incidence of false positives, providing more reliable data to decision-makers and optimizing the targeting of response actions.

4.2.2 Dispersion modeling

After confirmation of the detection, the numerical modeling module was activated. Using the modified MEDSLIK-II model, 72 hours of dispersion were simulated, considering medium-type oil, under oceanographic and meteorological conditions extracted from the Copernicus Marine Environment Monitoring Service (CMEMS) and ERA5. Figure 3 shows the temporal evolution of the oil plume, highlighting intervals from 9 to 50 hours after the initial detection.

The simulated trajectory (Figure 6) showed drift consistent with regional current and wind patterns, with displacement mainly to the west, following the direction of surface transport in the area. The plume remained cohesive until about 30 hours, at which point it began to elongate and fragment, indicating an intensification of diffusion and dispersion processes.

Figure 6 - Simulation of the dispersion of the stains identified by the system. Time interval between 9 and 50 hours after identification

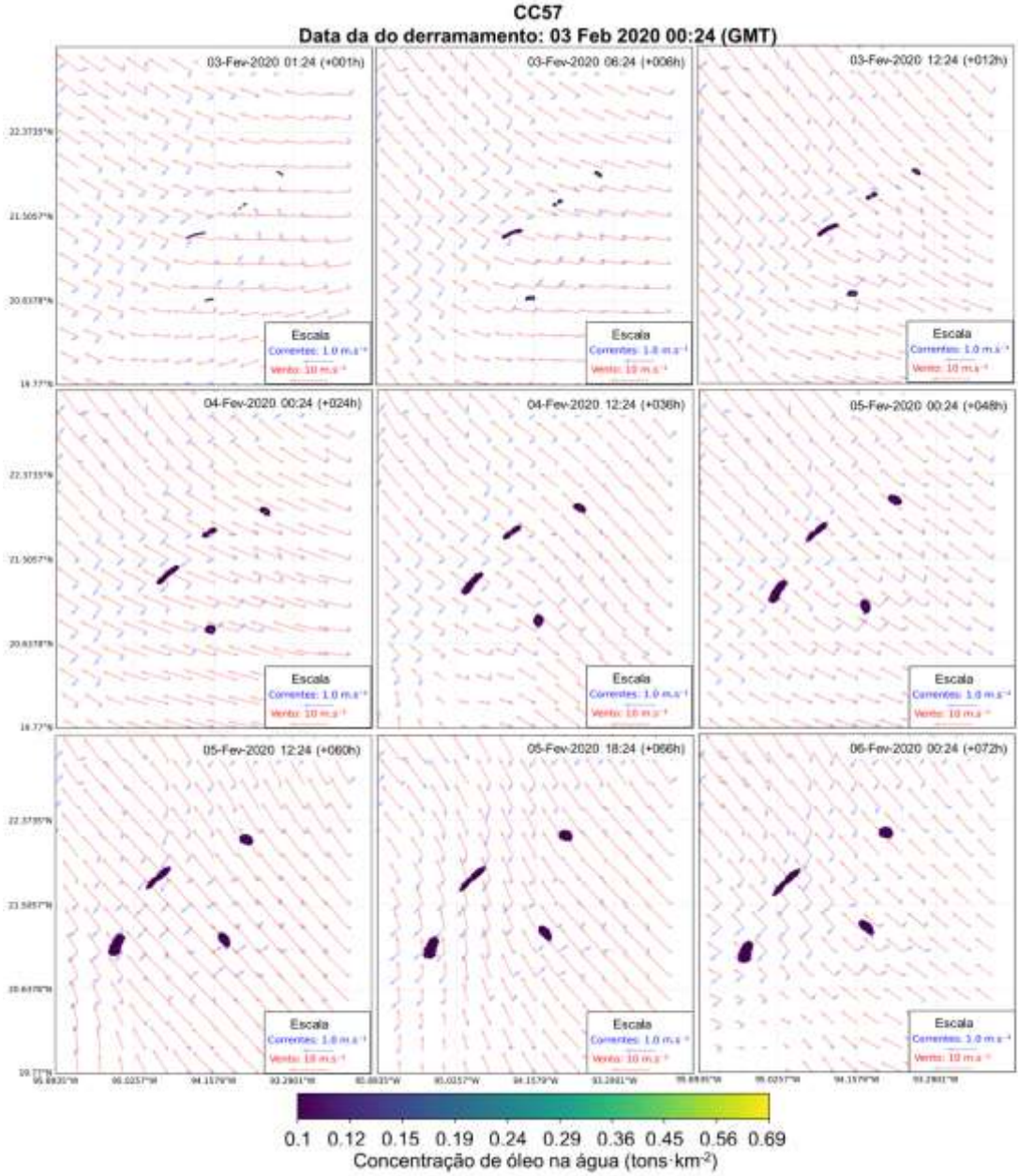

Source: MEDSLIK-II.

4.2.3 Operational analysis

This experiment serves as a basis for testing the system's ability to provide, in an integrated and autonomous manner, detection alerts and realistic projections of the spatial evolution of oil spills. The simulated data were exported in formats interoperable with GIS systems (NetCDF, GeoTIFF, and shapefiles), allowing overlay with socio-environmental layers and direct support for decision-making. Furthermore, the performance of the detection model and the consistency of the simulation with expected patterns demonstrate that the system is

applicable not only to historical events but also as a predictive tool in surveillance and rapid response operations.

4.3 CASE STUDY 2: NORTHCENTRAL PORTION OF THE GULF OF MEXICO

In order to demonstrate the applicability of the developed system in detecting oil targets on the ocean surface, with the presence of false positives, a detection episode located in the north-central portion of the Gulf of Mexico, south of the Louisiana coast (USA), was selected. This is an area quite close to offshore oil fields such as Mississippi Canyon and Green Canyon, regions historically associated with oil exploration, including near the site of the Deepwater Horizon disaster (2010), identified by Sentinel-1 SAR imagery.

Here we find an example of a spill surrounded by several cases of false positives such as low wind, close to the oil slick, and rain cells in the upper right corner of the image. This study illustrates the complete functioning of the SipamMAR operational chain, from image ingestion, through automatic detection, to dispersion simulation and visualization of potential impacts. Figure 7 represents the metadata of the analyzed image, with the boundary edges of the original satellite image.

Figure 7 – Metadata from the Sentinel-1 SAR image associated with the oil spill detected in the case study

Coord. Range	Minimum	Maximum
Latitude	27.9048	29.9471
Longitude	-91.1185	-88.203

- Input title: `S1A_IW_SLC__1SDV_20210805T000201_20210805T000228_039087_049CB9_D205`
- Input path: `/host/mnt/camobi_process/rioss_outputs/prod/data/76314c45-14f8-578c-8cda-4b47a6f908ca/preproc_sar/76314c45-14f8-578c-8cda-4b47a6f908ca.nc`

Source: SipamMar.

4.3.1 Automated detection

The analyzed SAR image was processed by the SipamMAR system, and the signaled alert was based on a RESNET-50 neural network, with pixel probability indices higher than those pre-established by the warning system. Figure 8 shows, on the left, the original SAR image and, on the right, the result of the semantic segmentation performed by the model, with the regions identified as oil highlighted in red. The analysis was conducted without human intervention, reinforcing the system's autonomy under real operating conditions.

Figure 8 - Imagens SAR D205. (a) Imagem SAR sem detecções; (b) Imagem SAR com as detecções do sistema, marcadas em vermelho

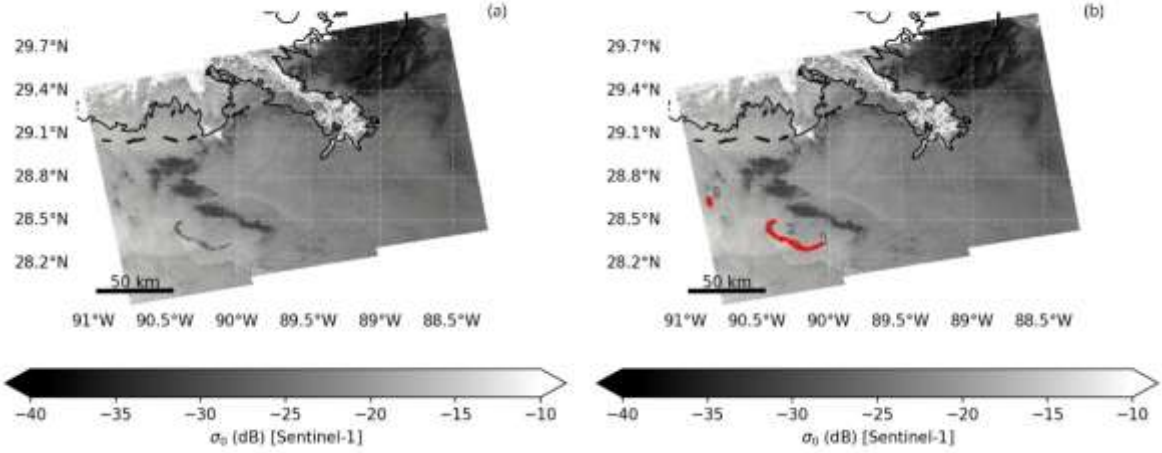

Source: SipamMar.

Figure 9 summarizes the results of oil spill segmentation in the ocean performed by the ResNet-50 convolutional neural network. Three identified polygons with different areas, geographic locations, and detection probabilities are observed. The first polygon, located at approximately 28.3185° longitude and -90.0854° latitude, has an area of 14.18 km², with a detection probability of 58% and a maximum probability of 85%. The second polygon is the largest, with 90.69 km², but has a lower probability (49%), although its estimated maximum is 86%. The third polygon, with only 9.56 km², has the lowest overall (41%) and maximum (80%) probabilities. These results suggest that, despite the consistency in identifying potentially contaminated regions, there is variability in both the spatial extent and the confidence attributed by the model to each detection.

The difference between the average and maximum probability can also indicate internal spatial heterogeneity within the segmented polygons. This pattern is consistent with the diffuse nature of oil slicks observed by remote sensing sensors, as well as with the classifier's limitations in handling transition areas and reduced spectral contrast. The presence of quicklook links facilitates visual verification and qualitative validation of these detections, reinforcing the integration between automated methods and human inspection in the environmental monitoring process.

Figure 9 – Metadata representing the output of the detection model with probability indices, estimated area, and geographic positioning

	Latitude	Longitude	Area (km²)	Probability	Highest Probability	Quicklook
1	-90.0854	28.3185	14.184	58%	85%	link
2	-90.3135	28.3824	90.689	49%	86%	link
3	-90.8336	28.6324	9.555	41%	80%	link

Source: SipamMar.

Figure 10 shows three automatic oil spill detection polygons processed in this case study by the SipamMar system. Each image shows the backscatter signature in decibels (σ_0), with the outlines of the segmented areas marked in red. Polygon 1 (Figure 1) displays a well-defined spill with an elongated structure, centered between 28.26°N and 28.38°N and with a sharp contrast in the σ_0 signature, reaching values below -30 dB, consistent with the suppression of scattering caused by oil films.

Polygon 2 (Figure 2), the largest in area (90,689 km²), presents a curved and extensive feature, with a more heterogeneous spatial distribution pattern and inserted in a hazy background field, which may indicate the presence of atmospheric interference or variations in surface roughness. Polygon 3 (Figure 3) is the smallest of the three, but it reveals a more fragmented and diffuse feature, suggesting oil dispersion or the presence of multiple point sources.

The coherence between the neural network (ResNet-50) contours and the low σ_0 areas reinforces the algorithm's effectiveness for the automatic detection of anomalies consistent with oil spills at sea, even in different morphological and spectral contexts. The visual interpretation, facilitated by the reflectivity scale and distance bars, corroborates the model's robustness in identifying potentially polluting events in oceanic environments.

Figure 10 - Excerpts of the oil slicks, from image D205, detected by the SipamMar system

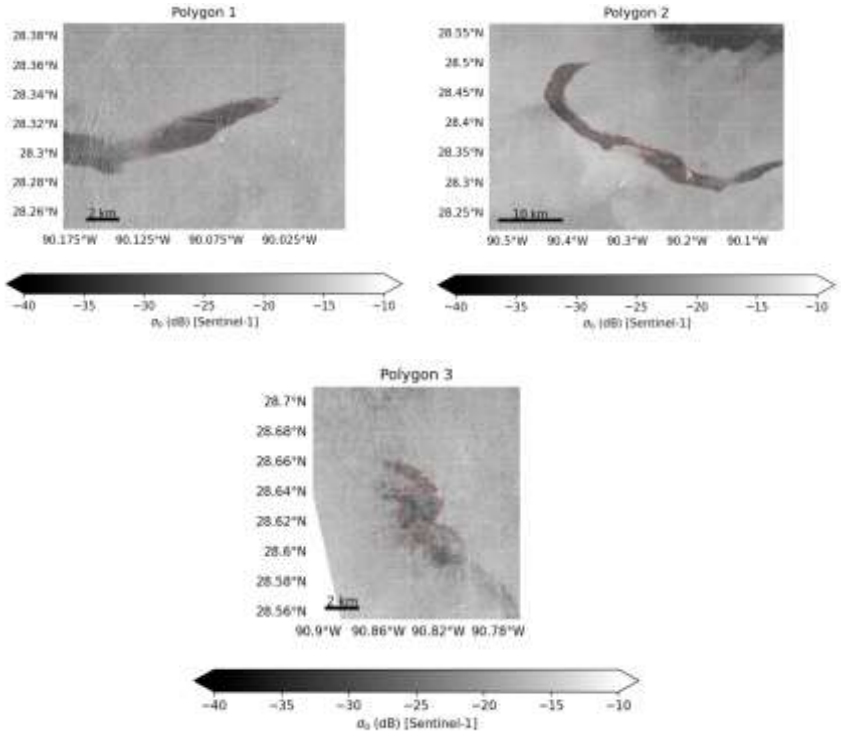

Source: SipamMar.

Figure 11 presents a set of auxiliary data used to support the operator's qualitative analysis in validating an automatic oil spill detection performed by the SipamMar system. The first subfigure shows the chlorophyll-a concentration (mg/m³), where it can be observed that the detected spill area has low levels of phytoplankton biomass, which reduces the possibility of biological fronts or spills of natural origin associated with intense biological activity. The second subfigure shows the surface wind field, evidencing moderate speeds (between 5 and 8 m/s) with a predominant north-south direction, consistent with the alignment and dispersion observed in the suspected feature, reinforcing the hypothesis of passive transport of an oily film.

Finally, the third subfigure shows the oil presence probability map generated by a classifier based on the U-Net architecture combined with ResNet-50, with values greater than 0.8 in the region of the spill, indicating high model confidence in the detection. The combination of these three informative layers—low chlorophyll, wind vector coherence, and high probability—provides a robust basis for confirming the anomaly as a potential oil spill and recent methodological updates applied to artificial intelligence in environmental remote sensing.

Figure 11 – Auxiliary data for predicting oil detection, with maps of surface chlorophyll concentration, wind speed, and the oil probability map associated with the prediction models

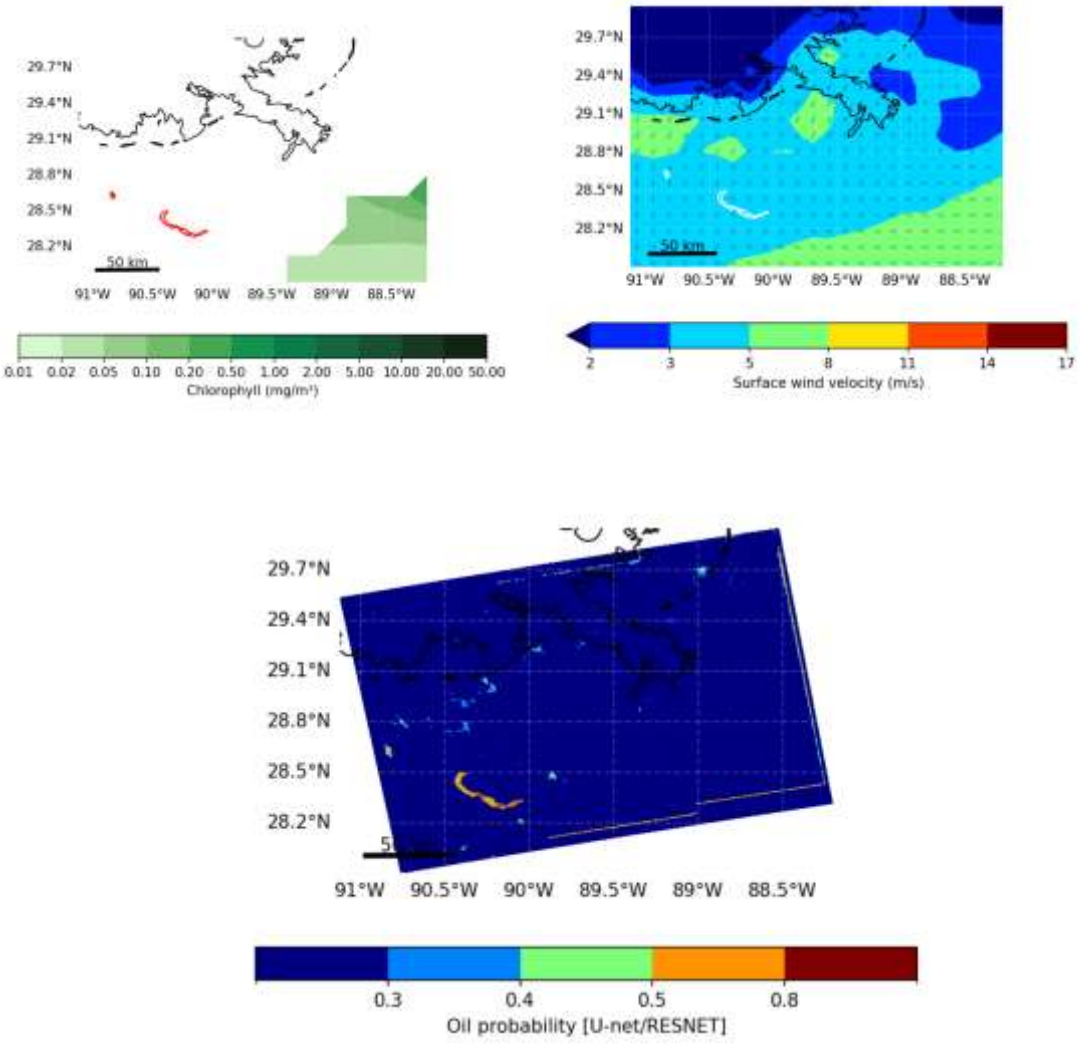

Source: SipamMar.

4.3.2 Dispersion modeling

After confirmation of the detection, the numerical modeling module was activated. Using the modified MEDSLIK-II model, 72 hours of dispersion were simulated, considering medium-type oil, under oceanographic and meteorological conditions extracted from the Copernicus Marine Environment Monitoring Service (CMEMS) and ERA5. Figure 9 shows the temporal evolution of the oil plume, highlighting intervals from 9 to 50 hours after the initial detection.

Figure 12 simulates the trajectory and evolution of the oil concentration on the sea surface from a spill event that occurred on August 5, 2021. Each panel represents a time instant, in increments of six hours up to 72 hours after the initial event, revealing the dynamic behavior

of the slick under the combined action of ocean currents (blue vectors) and surface winds (red vectors). The oil slick is represented in shades of purple to yellow, corresponding to the concentration of oil in tons per square kilometer, with the highest values (above 5.66 $t.km^{-2}$) indicated by the lighter shades.

Throughout the simulation, a gradual displacement of the oil slick from west to east-northeast is observed, consistent with the local ocean circulation and the overlying wind field. This pattern highlights the influence of the cyclonic current's rotation in the region and the action of the wind as a secondary driving force, contributing to the transport and deformation of the slick. Numerical predictions show that, in about three days, the slick travels a significant distance, modifying its shape and concentration distribution, which is crucial for assessing environmental impacts and prioritizing responses in sensitive coastal areas or areas of economic activity.

Models like MEDSLIK-II are fundamental tools in the context of responding to environmental emergencies involving oil spills. By integrating remote sensing data with environmental forecasting (wind and current), these models allow for the estimation of the likely trajectory of the oil spill in near real-time, providing technical support for operational decisions, such as the mobilization of containment vessels, the direction of absorption buoys, or the issuance of alerts to coastal communities. Automatic simulation from central points detected by the SipamMar system represents an advance in the automation of monitoring and response, aligning artificial intelligence with predictive modeling in an integrated and efficient approach to environmental disaster management.

Figure 12 – Simulation of oil spill dispersion performed with the MEDSLIK-II model for the event detected on August 5, 2021, at 00:02 GMT (case D250). The panels show the evolution of the surface oil concentration (tons·km^{-2}) over 72 hours, at regular 6-hour intervals

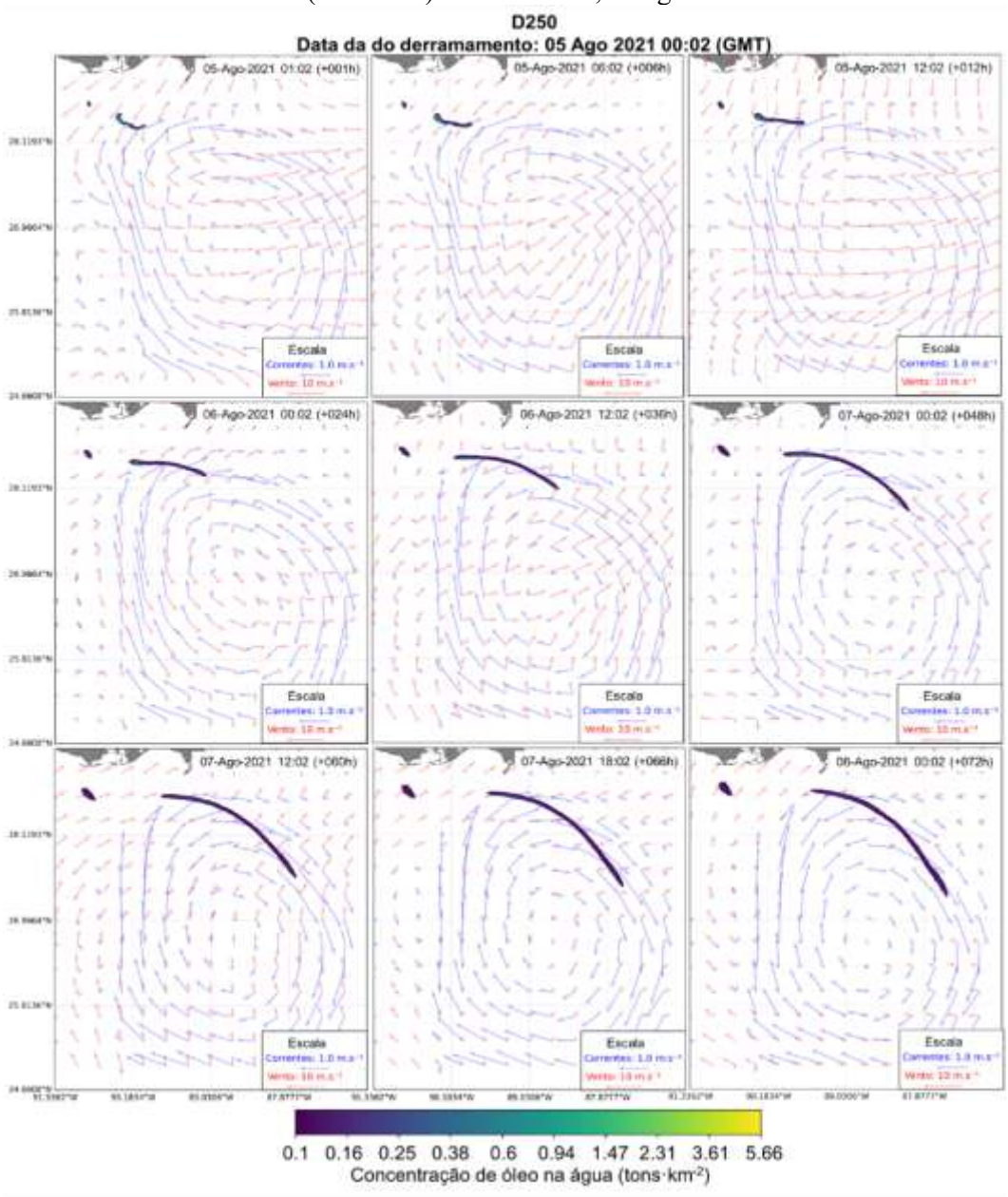

Source: MEDSLIK-II

5 CONCLUSION

The development and implementation of the SipamMAR system represent a significant advancement in the national capacity for environmental monitoring and response to oil spills in Brazilian jurisdictional waters. By integrating SAR remote sensing technologies, deep learning algorithms with convolutional neural networks, and numerical modeling of contaminant

dispersion, the system automates the detection, alert, and forecasting chain, reducing dependence on human actions and optimizing operational efficiency.

The performance of a convolutional neural network in detecting oil slicks in SAR images is intrinsically linked to environmental conditions that influence the backscattering of radar waves on the ocean surface. Factors such as wind speed and direction, for example, are fundamental. Strong winds increase surface roughness, raising overall backscattering and potentially masking the slick, while weak winds can create natural dark patches that can be mistaken for oil, leading to false positives. Furthermore, the concentration of biogenic films, such as chlorophyll, also has the potential to create natural dark patches for SAR sensors and, therefore, the potential to generate false positives.

It was observed that in situations of weak wind, the convolutional network maintained a high detection rate, with average confidence levels higher than the observed average, reflecting the good spectral separability of oil patterns in contrast to calm seas. On the other hand, in conditions with the presence of lookalikes (e.g., algal blooms, thermal fronts, and shear zones), the false positive rate increased by approximately 12–15%, reducing the average confidence level to values higher than those expected by different references cited in the work. This variation indicates that the network is more sensitive to complex surface features than to isolated meteorological conditions.

We also highlight that the consistency with auxiliary data (wind and surface currents) contributed to reducing uncertainty: when associated with oceanographic situations consistent with oil spills (e.g., advection aligned with the prevailing wind), the probability of correct detection was higher. This analysis suggests that future versions of the system could be improved by explicitly integrating environmental variables as additional inputs to the model, increasing its robustness against lookalikes and adverse conditions.

Case studies demonstrate the robustness of the U-Net and ResNet-50 classifiers in segmenting oil spills in SAR images, with consistent performance even in complex environments subject to interference, such as regions with lookalikes or adverse weather conditions. The integration of auxiliary data, such as wind fields, chlorophyll concentration, and detection probabilities, proved essential for reducing false positives and validating the detected anomalies.

This multivariate approach strengthens decision-making and contributes to a faster and more informed response. In turn, predictive modeling with MEDSLIK-II, automatically fed by high-resolution observational and predictive data, allows for the simulation of realistic oil

transport and transformation scenarios, providing fundamental technical support for the actions of environmental agencies, maritime authorities, and port operators.

Despite the progress achieved, it is important to acknowledge some limitations of this study. We emphasize that systematic statistical validation of the automatic detections, based on in situ test events, was not conducted. We believe this restricts the quantification of classifier performance in varied real-world scenarios. To overcome this problem, we have a group of trained operators to verify each warning signal from the system. Another important aspect to consider is the predominance of the use of simulated data or specific case studies, still lacking broad and continuous real-time operational application. This will allow SipamMar to assess the system's robustness against different types of oil and marine biomes.

As future perspectives, we highlight the expansion of the training database with data from multiple sensors, the integration of statistical validation routines comparing automatic detections with field observations, and the testing of the platform in different coastal and oceanic environments. Furthermore, the incorporation of SipamMar into governmental emergency response protocols could enhance its practical impact, expanding support for monitoring and mitigating oil spills in Brazilian jurisdictional waters.

Given the challenges posed by the vastness of the Blue Amazon and the increasing anthropogenic pressure on marine ecosystems, SipamMAR offers an autonomous, scalable, and highly strategic technological alternative. By consolidating the application of artificial intelligence and environmental modeling in the context of ocean surveillance, the system is configured as a state tool for the protection of marine resources, reinforcing national sovereignty, environmental security, and the capacity to respond to large-scale ecological disasters.

The system represents a significant advance in Brazil's capacity to respond to environmental incidents at sea, especially by integrating different data sources, process automation, and spatial visualization to support decision-making. It is expected that, with continued development and the incorporation of new functionalities, such as environmental impact indices and an integrated web interface, the system can be consolidated as a strategic solution for the protection of the Blue Amazon and the country's coastal zones.

REFERENCES

AGHAEI, N.; AKBARIZADEH, G.; KOSARIAN, A. Osdes_net: oil spill detection based on efficient_shuffle network using synthetic aperture radar imagery. **Geocarto International**, Abingdon, v. 37, n. 26, p. 13539–13560, 25 May 2022. Available at: DOI: https://doi.org/10.1080/10106049.2022.2082545. Accessed on: 7 July 2025.

ANDRADE, I. O.; FRANCO, L. G. A. A Amazônia Azul como fronteira marítima do Brasil: importância estratégica e imperativos para a defesa nacional. *In:* PÊGO, B.; MOURA, R. (Org.). **Fronteiras do Brasil: uma avaliação de política pública**. v. 1. Rio de Janeiro: Ipea; MI, 2018. p. 151–177.

BARBOSA JÚNIOR, I. Oceanopolítica: conceitos fundamentais Amazônia Azul. *In:* MORE, R. F.; BARBOSA JÚNIOR, I. (Org.). **Amazônia Azul: política, estratégia e direito para o Oceano do Brasil**. Rio de Janeiro: FEMAR, 2012. p. 205–231.

BEIRÃO, A.; MARQUES, M.; RUSCHEL, R. R. **O valor do mar: uma visão integrada dos recursos do oceano do Brasil**. São Paulo: Essential Idea Editora, 2020. 248 p.

BREKKE, C.; SOLBERG, A. H. S. Oil spill detection by satellite remote sensing. **Remote Sensing of Environment**, New York, v. 95, n. 1, p. 1-13, 2005. DOI: https://doi.org/10.1016/j.rse.2004.11.015. Accessed on: 3 June 2025.

BHATTACHARYYA, S. et al. **Deep learning: research and applications**. Berlin; Boston: De Gruyter, 2020. p.1-19. DOI: https://doi.org/10.1515/9783110670905. Accessed on: 01 June 2025.

CHEN, G. *et al.* Application of deep networks to oil spill detection using polarimetric synthetic aperture radar images. **Applied Sciences**, Basel, v. 7, n. 10, p. 968, 21 set. 2017. DOI: https://doi.org/10.3390/app7100968. Accessed on: 05 June 2025.

CORREIA LIMA, E. J. A. *et al.* The effect of wind parametrizations in MEDSLIK-II oil spill simulations: a case study of the FPU P-53 incident in Brazilian waters. **Marine Pollution Bulletin**, v. 218, May 2025, *article* 118118. DOI: https://doi.org/10.1016/j.marpolbul.2025.118118.

DOMINICIS, M. DE *et al.* MEDSLIK-II, a Lagrangian marine surface oil spill model for short-term forecasting – Part 2: Numerical simulations and validations. **Geoscientific Model Development**, 1 nov. 2013. v. 6, n. 6, p. 1871–1888. DOI: https://gmd.copernicus.org/articles/6/1871/2013/. Accessed on: 19 June 2025.

DOMINICIS, M. DE *et al.* MEDSLIK-II, a Lagrangian marine surface oil spill model for short-term forecasting – Part 1: Theory. **Geoscientific Model Development**, 1 nov. 2013. v. 6, n. 6, p. 1851–1869. Available at: https://gmd.copernicus.org/articles/6/1851/2013/. Accessed on: 17 June 2025.

DE MOURA, W. S. G.; POLITO, P. O. S. The 2019 northeast Brazil oil spill: scenarios. **Anais da Academia Brasileira de Ciências**, Rio de Janeiro, v. 94, n. 2, e20210532, 2022. DOI: https://doi.org/10.1590/0001-3765202220210391. Accessed on: 2 June 2025.

HASSELMANN, K. *et al*. Measurements of wind-wave growth and swell decay during the Joint North Sea Wave Project (JONSWAP). **Deut. Hydrogr. Z.**, v. 8, p. 1–95, 1 jan. 1973.

LEMLEY, J.; BAZRAFKAN, S.; CORCORAN, P. Deep learning for consumer devices and services: pushing the limits for machine learning, artificial intelligence, and computer vision. **IEEE Consumer Electronics Magazine**, Piscataway, v. 6, n. 2, p. 48–56, 1 abr. 2017. DOI: https://doi.org/10.1109/mce.2016.2640698. Accessed on: 20 May 2025.

LIU, P.; ZHAO C.; LI, X.; HE, M.; PICHEL, W. Identification of ocean oil spills in SAR imagery based on fuzzy logic algorithm. **International Journal of Remote Sensing**, Abingdon, v. 31, n. 17–18, p. 4819–4833, 20 set. 2010. DOI: https://doi.org/10.1080/01431161.2010.485147. Accessed on: 12 May 2025.

MACKAY, D.; PATERSON, S.; TRUDEL, K. **A mathematical model of oil spill behaviour**. Report to Research and Development Division, Environment Emergency Branch, Environmental Impact Control Directorate. Ottawa: Environmental Protection Service, Environment Canada, 1980.

MAGRIS, R. A.; GIARRIZZO, T. Mysterious oil spill in the Atlantic Ocean threatens marine biodiversity and local people in Brazil. **Marine Pollution Bulletin**, Kidlington, v. 153, 110961, 2020. DOI: https://doi.org/10.1016/j.marpolbul.2020.110961. Accessed on: 13 May 2025.

MITYAGINA, M.; LAVROVA, O. Oil slicks from natural hydrocarbon seeps in the Southeastern Black Sea, their drift and fate as observed via remote sensing. *In:* INTERNATIONAL GEOSCIENCE AND REMOTE SENSING SYMPOSIUM (IGARSS), 2018, Valencia. **Anais** […]. Piscataway: IEEE, 2018. p. 7926–7929. DOI: https://doi.org/10.1109/IGARSS.2018.8517607. Accessed on: 9 June 2025.

NIRCHIO, F. *et al*. Automatic detection of oil spills from SAR images. **International Journal of Remote Sensing**, Abingdon, v. 26, n. 6, p. 1157–1174, 1 mar. 2005. DOI: https://doi.org/10.1080/01431160512331326558. Accessed on: 26 May 2025.

ORTIZ VALADEZ, S. C. *et al*. **Languages with artificial intelligence applications**. Hershey: IGI Global, 2024. p. 192–201. DOI: https://doi.org/10.4018/979-8-3693-1119-6.ch010. Accessed on: 27 May 2025.

PESSOA, J. C. O. **Estudo mineralógico e geoquímico de crostas polimetálicas (FeMn-Co) das áreas Alpha e Bravo da Elevação do Rio Grande**. 2015. 83 f. Dissertação (Mestrado) – Universidade Estadual de Campinas, Campinas, 2015. Available at: https://rigeo.sgb.gov.br/handle/doc/16018. Accessed on: 13 May 2025.

RAEISI, A.; AKBARIZADEH, G.; MAHMOUDI, A. Combined method of an efficient cuckoo search algorithm and nonnegative matrix factorization of different Zernike moment features for discrimination between oil spills and lookalikes in SAR images. **IEEE Journal of Selected Topics in Applied Earth Observations and Remote Sensing**, Piscataway, v. 11, n. 11, p. 4193–4205, 1 nov. 2018. DOI: https://doi.org/10.1109/jstars.2018.2841503. Accessed on: 7 July 2025.

SILVA, A. P. S. Brazil advances over the Area: the inclusion of the Rio Grande Rise within the Brazilian outer continental shelf and its consequences for other states and for the common

heritage of mankind. **Marine Policy**, Oxford, v. 125, 104399, 2021. DOI: https://doi.org/10.1016/j.marpol.2021.104399. Accessed on: 05 June 2025.

SOARES, M. O. et al. The most extensive oil spill registered in tropical oceans (Brazil): the balance sheet of a disaster. **Environmental Science and Pollution Research**, Berlin, v. 29, p. 14598–14611, 2022. DOI: https://doi.org/10.1007/s11356-022-18710-4. Accessed on: 10 June 2025.

TOPOUZELIS, K. N. Oil spill detection by SAR images: dark formation detection, feature extraction and classification algorithms. **Sensors**, Basel, v. 8, n. 10, p. 6642–6659, 23 out. 2008. DOI: https://doi.org/10.3390/s8106642. Accessed on: 20 June 2025.

ZAKZOUK, M.; ABDULAZIZ, A. M.; ABOU EL-MAGD, I. *et al.* Automated oil spill detection using deep learning and SAR satellite data for the northern entrance of the Suez Canal. **Scientific Reports**, London, v. 15, article 20107, 2025. DOI: https://doi.org/10.1038/s41598-025-03028-1. Accessed on: 26 June 2025.

ZHOU, Z.; RAHMAN SIDDIQUEE, M. M.; TAJBAKHSH, N.; LIANG, J. UNet++: a nested U-net architecture for medical image segmentation. In: STOYANOV, D. et al. (Org.). **Deep learning in medical image analysis and multimodal learning for clinical decision support.** Cham: Springer, 2018. (Lecture Notes in Computer Science, v. 11045). p. 3–11. DOI: https://doi.org/10.1007/978-3-030-00889-5_1.